Crystal and electronic structure of a quasi-two-dimensional semiconductor $Mg_3Si_2Te_6$

Chaoxin Huang(黄潮欣)[1,†], Benyuan Cheng(程本源)[2,3,†], Yunwei Zhang(张云蔚)[1], Long Jiang(姜隆)[4], Lisi Li(李历斯)[1], Mengwu Huo(霍梦五)[1], Hui Liu(刘晖)[1], Xing Huang(黄星)[1], Feixiang Liang(梁飞翔)[1], Lan Chen(陈岚)[1], Hualei Sun(孙华蕾)[1], and Meng Wang(王猛)[1,‡]

[1] *Center for Neutron Science and Technology, Guangdong Provincial Key Laboratory of Magnetoelectric Physics and Devices, School of Physics, Sun Yat-Sen University, Guangzhou* 510275, *China*

[2] *Shanghai Institute of Laser Plasma, Shanghai* 201800, *China*

[3] *Center for High Pressure Science and Technology Advanced Research, Shanghai* 201203, *China*

[4] *Instrumentation Analysis and Research Center, Sun Yat-Sen UniVersity, Guangzhou* 510275, *China*

(Received 31 August 2022; revised manuscript received 28 October 2022; accepted manuscript online 17 November 2022)

We report the synthesis and characterization of a Si-based ternary semiconductor $Mg_3Si_2Te_6$, which exhibits a quasi-two-dimensional structure, where the trigonal $Mg_2Si_2Te_6$ layers are separated by Mg ions. Ultraviolet-visible absorption spectroscopy and density functional theory calculations were performed to investigate the electronic structure. The experimentally determined direct band gap is 1.39 eV, consistent with the value of the density function theory calculations. Our results reveal that $Mg_3Si_2Te_6$ is a direct gap semiconductor, which is a potential candidate for near-infrared optoelectronic devices.

Keywords: semiconductors, semiconductor compounds, narrow-band systems, methods of crystal growth

PACS: 78.40.Fy, 71.20.Nr, 71.28.+d, 81.10.–h **DOI:** 10.1088/1674-1056/aca393

1. Introduction

Semiconductors play an important role in optoelectronic and magnetic devices. The properties and applications of semiconductors have been widely studied for decades in a variety of fields, such as magnetic field sensors, photovoltaics, infrared photodetectors, lasers and so on.[1–5] Magnetic field sensors, including magnetoresistors and Hall sensors, are generally used in magnetic recording and magnetic measurement technologies.[6,7] Materials for magnetic field sensors are doped semiconductors with high electronic density of states and mobility, such as InSb and InAs which are extremely sensitive to magnetic field.[8–10] Conventional photovoltaic materials mostly use wide-gap semiconductors that utilize photons in the ultraviolet and visible regions, limiting the conversion efficiency. Tuning the band gap is considered to be one of the effective solutions.[11] Narrow-gap semiconductor-based photoelectrodes can absorb light at longer wavelengths and enhance the solar energy conversion efficiency.[12] The narrow-gap semiconductors are also important for lasers due to their stability, tunability, and simple structures.[13,14] As a more widely used field, infrared photodetectors, such as the quantum dots-in-a-well photodetectors, have developed rapidly in recent years.[15–17]

Compared with visible and ultraviolet light, near-infrared (NIF) photons exhibit greater tissue penetration depth, which expands the application of NIF optoelectronic materials.[18–20] One of the most important parameters for optoelectronic materials is the electronic band gap. $Hg_{1-x}Cd_xTe$ and $Pb_{1-x}Sn_xTe$ are among the hottest researched semiconducting systems in recent years, whose gaps can be tuned by compositions in a wide range, from NIF energy to even close to zero.[14,21–23] Although HgCdTe and InGaAs based detectors have been well available in commercial applications, their poor flexibility, instability of the material interface, complex manufacturing process, and low temperature working environment limit their further development.[24–26] Therefore, it is crucial to search for more semiconductors that are suitable for manufacturing stable and efficient infrared detectors. Meanwhile, new semiconductors with excellent performance also have potential applications in laser, photovoltaics, and other magnetic devices.

In this work we report the successful synthesis of a Si-based nonmagnetic semiconductor $Mg_3Si_2Te_6$, whose structure is found to exhibit a quasi-two-dimensional (quasi-2D) layered configuration. Fittings using direct and indirect band gap models to the ultraviolet-visible (UV-vis) absorption spectra result in a direct gap of 1.39 eV or an indirect gap of 0.6 eV, respectively. Electronic structure calculations using density functional theory (DFT) yield a direct band gap of 1.2 eV, close to the direct gap fitted from the UV-vis absorption spectra, revealing that $Mg_3Si_2Te_6$ is a direct gap semiconductor. The band gap is narrower than the energies of visible photons, allowing $Mg_3Si_2Te_6$ a potential candidate for NIF optoelectronic material.

[†] The authors contributed equally to this work.

[‡] Corresponding author. E-mail: wangmeng5@mail.sysu.edu.cn

© 2023 Chinese Physical Society and IOP Publishing Ltd

2. Experiment and calculation

Single crystal samples of $Mg_3Si_2Te_6$ were grown by a self-flux method.[27–29] Mg (99.99%) robs, Si (99.99%) powders, and Te blocks (99.99%) were mixed in a molar ratio of 3 : 2 : 6 after rough grinding, then sealed in an evacuated quartz ampoule. The ampoule was firstly heated to 600 °C in 10 h and held for 15 h, then heated to 1050 °C in 20 h and dwelled for 10 h, followed by a slow cooling to 750 °C in 150 h before the furnace was shut down. Shiny plate-like single crystals were obtained. The samples are air sensitive and were stored in an argon-filled glove box to minimize the exposure to air.

Single-crystal x-ray diffraction (XRD) measurements on a single-crystal x-ray diffractometer (SuperNova, Rigaku), a scanning electron microscopy (SEM) photography, and an energy dispersive x-ray spectroscopy (EDS) (EVO, Zeiss) were employed to determine the crystal structure, morphology and composition. Resistivity was measured using the standard four-probe method on single crystals with a typical size of 3 $\times 1 \times 0.5$ mm^3 on a physical property measurement system (PPMS) (Quantum Design). UV-vis absorption spectroscopy measurements were conducted using an Ocean Optics DH-2000-BAL spectrometer. The sample was pre-peeled into thin flakes with a thickness of $\sim$ 15 μm and then loaded into a diamond anvil cell (DAC) to avoid oxidation. The outboard ring of the DAC is the T301 steel gasket, which was pre-indented and a hole with a diameter of 150 μm was drilled to serve as the sample chamber. Each spectrum was collected for 2 s with wavelengthes ranged from 180 nm to 860 nm. The signal from background was obtained by shining the beam on a spot inside the sample chamber but away from the sample.

Electronic band structure was calculated using the DFT within the Perdew–Burke–Ernzerhof (PBE) exchange–correlation as implemented in the Vienna *Ab initio* simulation package (VASP) code.[30,31] A plane wave energy cutoff of 600 eV and dense meshes of Monkhorst–Pack k-points were used to ensure that all calculations are well converged to 1 meV/atom.

3. Results and discussion

The structure of $Mg_3Si_2Te_6$ is refined from XRD measurements on single crystals. $Mg_3Si_2Te_6$ crystalizes in the trigonal space group $P\bar{3}1c$ with $a = 7.0642(9)$ Å and $c = 14.464(2)$ Å at 253 K and exhibits a quasi-2D structure. The measured structure factors match the calculated structure factors well as shown in Fig. 1. The structural parameters are summarized in Table 1. The crystal structures viewed from different directions are illustrated in Fig. 2. The layer of the *ab* plane constituting the formula as $Mg_2Si_2Te_6$ consists of edge shared $MgTe_6$ octahedra and Si–Si dimers. The $Mg_2Si_2Te_6$ layer is isomorphic to a widely studied 2D van der Waals ferromagnetic compound $Cr_2Si_2Te_6$.[32,33] The layers are linked by Mg_2 that is half of Mg_1, constituting $Mg_3Si_2Te_6$. $Mg_3Si_2Te_6$ is isostructural to $Mn_3Si_2Te_6$[34] and $Mn_3Si_2Se_6$[35] which are quasi-2D semiconductors with enriched properties such as ferrimagnetism and large colossal magnetoresistance.[36,37]

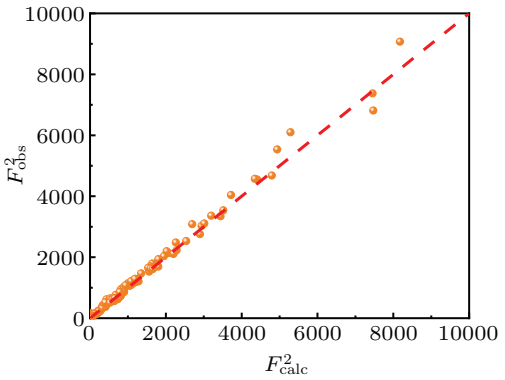


Fig. 1. Comparison of the calculated and measured structure factors for a single crystal of $Mg_3Si_2Te_6$.

Table 1. Parameters of $Mg_3Si_2Te_6$ refined from single-crystal XRD at 253 K.

Empirical formula	$Mg_3Si_2Te_6$
Formula weight	894.69
Temperature	252.99(10) K
Crystal system	trigonal
Space group	$P\bar{3}1c$
Unit-cell parameters	$a = b = 7.0642(9)$ Å
	$c = 14.464(2)$ Å
	$\alpha = \beta = 90°$
	$\gamma = 120°$
Atomic parameters	
Mg_1	4*f* (1/3, 2/3, 0.4987(5))
Mg_2	2*d* (2/3, 4/3, 1/4)
Si	4*e* (0, 1, 0.4192(4))
Te	12*i* (*x*, *y*, *z*)
	$x = 0.3402(1)$, $y = 0.9990(2)$,
	$z = 0.3733(1)$
Volume	625.11(18) Å^3
Density	4.753 g/cm^3
Absorp. coeff.	14.102 mm^{-1}
$F(000)$	725.0
Crystal size	0.09 × 0.04 × 0.02 mm^3
Radiation	Mo K_α ($\lambda = 0.7107$ Å)
2Θ range for data collection	5.632° to 53.96°
Index ranges	$-9 \le h \le 7$, $-9 \le k \le 9$,
	$-18 \le l \le 18$
Reflections collected	3733
Independent reflections	439
Data/restraints/parameters	439/0/18
Goodness-of-fit on F^2	0.904
Final R indexes [$I \ge 2\sigma(I)$]	$R_1 = 0.0391$, $wR_2 = 0.0790$
Final R indexes [all data]	$R_1 = 0.0767$, $wR_2 = 0.1014$
Largest diff. peak/hole (e·Å^{-3})	1.38/−0.96

To determine the composition of the samples, we performed EDS measurements on $Mg_3Si_2Te_6$ single crystals. Figure 3(a) is a zoomed-in view of the measured crystal in the *ab* plane taken from SEM. By normalizing the content

of Mg to be 3, the composition determined from EDS is $Mg_3Si_{1.87(4)}Te_{6.8(2)}$. The ratio of Mg to Si ratio is close to the expectation. The exceeding content of Te of 13% may be attributed to the excess Te flux on the surface.

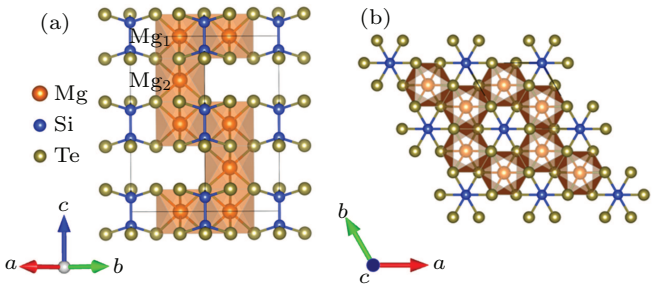


Fig. 2. Crystal structure of $Mg_3Si_2Te_6$ (space group: $P\bar{3}1c$) viewed (a) perpendicular to the c-axis and (b) parallel to the c-axis, respectively. The orange, blue, and grey balls represent Mg, Si, and Te.

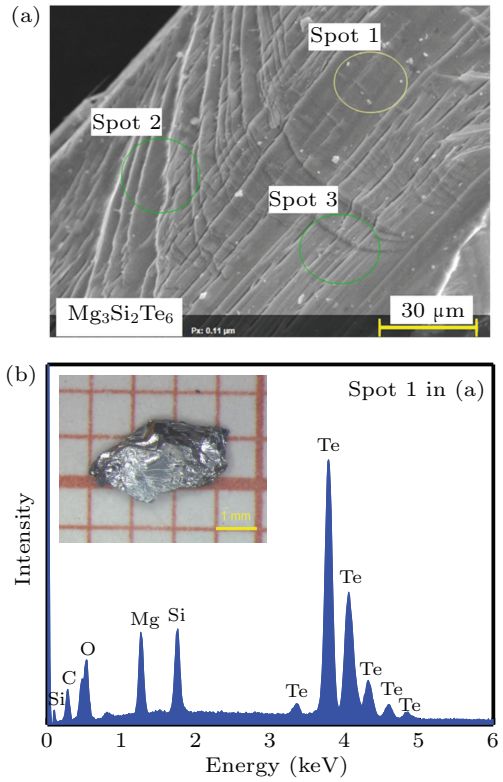


Fig. 3. (a) A zoomed-in view on the surface of the $Mg_3Si_2Te_6$ single crystal taken from SEM. The three circles mark the measured spots. (b) An EDS spectrum of the spot 1 in (a). The elements represented by different characteristic peaks are indicated. Small amounts of carbon and oxygen may derive from the background of conductive adhesive tape. The inset is a photo of the single crystal under an optical microscope.

Figure 4 shows the resistivity measured between 328 K and 400 K. The resistivity below 328 K exceeding 10^6 Ω·cm is beyond the measured range of the instrument. As shown in Fig. 4(a), the resistivity exhibits an insulating behavior, and no obvious anomaly can be observed up to 400 K. Figure 4(b) is a plot of the resistivity in $\ln\rho$ as a function of $1000/T$. A fitting using the thermal activation-energy model $\rho(T) = \rho_0 \exp(E_a/k_B T)$ to the linear segment that corresponds to 350 K to 400 K results in $E_a = 0.378$ eV. In the model, ρ_0 is a prefactor, k_B is the Boltzmann constant, and E_a is the thermal activation energy. The obtained activation energy of 0.378 eV indicates that the energy gap of $Mg_3Si_2Te_6$ may be narrower than that of visible light of 1.64–3.19 eV. We note that the fitted thermal activation energy at 350–400 K may be much smaller than the band gap at low temperature.

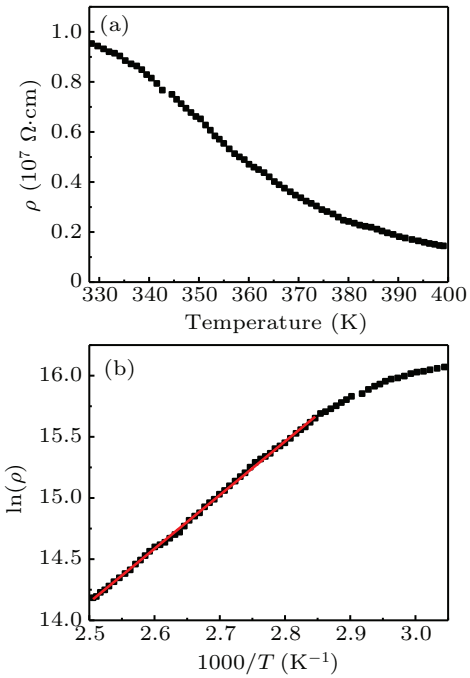


Fig. 4. (a) Resistivity of $Mg_3Si_2Te_6$ in the temperature range of 328–400 K. (b) $\ln\rho$ as a function of $1000/T$. The red line is a fitting using the thermal activation-energy model $\rho(T) = \rho_0 \exp(E_a/k_B T)$.

UV-vis absorption spectra were employed to study the electronic band gap of $Mg_3Si_2Te_6$. Five spots on a single crystal were measured separately. The thickness of the single crystal $\sim$ 15 μm used in the UV-vis absorption measurements will not affect the band gap as previous measurements on 2D semiconductors.[38,39] The absorption spectra are shown in Fig. 5(a), yielding a typical semiconducting state with a strong absorption in the range of 700–860 nm, while the rest of the short wavelength data are removed because of relatively high noise. The band gap can be obtained by fitting the absorption spectra using the Tauc relation, that is, $[F(R_\infty)h\nu]^{1/n} = A(h\nu - E_g)$, where $F(R_\infty)$ is the Kubelka–Mubelka–Munk function, h is the Planck constant, ν is the frequency, A is a prefactor, and E_g is the band gap energy.[40] For a direct band gap semiconductor, n is 1/2; for an indirect band gap semiconductor, n is 2. We plot the Tauc relations as a direct gap and indirect gap semiconductor in Figs. 5(b) and 5(c), respectively. The size of the band gap is extracted from the linear regression at the inflection point and the obtained $h\nu$-intercept value is taken as the band gap value.[41] The measured absorption spectra could not distinguish the two models due to poor statistic. We fitted the linear parts of five sets of data by adopting the Tauc relation and $n = 1/2$, resulting in

the direct band gaps of 1.41 eV, 1.43 eV, 1.43 eV, 1.37 eV, and 1.31 eV. Thus, the direct gap is estimated to be 1.39(5) eV by averaging the fitted values. Following the same procedure and adopting $n = 2$, an indirect band gap of 0.6(2) eV is obtained. The difference in the calculated energy gaps between different data sets may be attributed to the inconsistency of the transmittance and reflectivity of the samples to ultraviolet light.

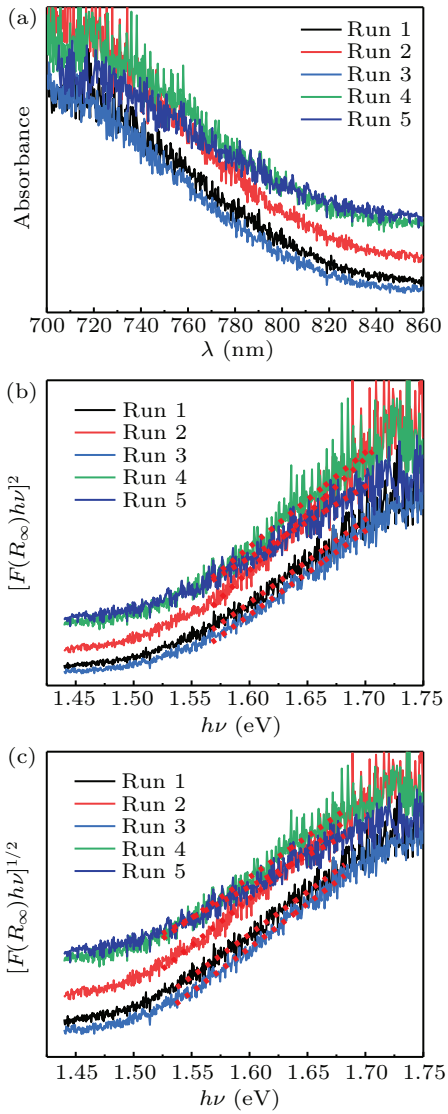


Fig. 5. (a) UV-vis absorption spectra of $Mg_3Si_2Te_6$ in a DAC at room temperature. (b) The Tauc plots of $[F(R_\infty)h\nu]^{1/n} = A(h\nu - E_g)$ versus $h\nu$ with $n = 1/2$ for direct band gap and (c) $n = 2$ for indirect band gap. The dotted red lines are fittings of the linear regions.

In order to distinguish the direct gap and indirect gap from the fittings of the UV-vis absorption spectra, DFT calculations were performed to investigate the electronic band structure. Figure 6 displays the band structures along high symmetry directions in a Brillouin zone and partial density of states (PDOS) of $Mg_3Si_2Te_6$. The calculated data reveal a direct gap of ~ 1.2 eV at the Γ point, close to the fitting results from the UV-vis absorption spectra using the direct gap model. Thus, $Mg_3Si_2Te_6$ can be considered as a direct gap semiconductor with a gap size of 1.2–1.39 eV. This value is larger than the thermal activation energy of 0.378 eV fitted from the resistivity between 350 K and 400 K. The outcomes may be ascribed to the fact that the activation energy is fitted from the resistance change at high temperature, where thermal fluctuations increase the electron hopping capability, and the gap seems to be narrowed. The direct gap size of $Mg_3Si_2Te_6$ is smaller than the energies of visible light. Through doping, temperature, and pressure, the band gap of $Mg_3Si_2Te_6$ may be further decreased, allowing $Mg_3Si_2Te_6$ as one of the potential candidates for NIF optoelectronic materials.

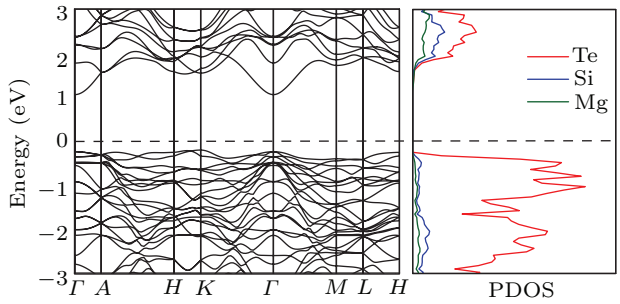


Fig. 6. Electronic structure calculation using DFT. The direct gap of $Mg_3Si_2Te_6$ is about 1.2 eV. PDOS is obtained by integrating density states of the energy bands, and the electrons close to the Fermi surface are mainly provided by Te.

4. Summary

In conclusion, we synthesized single crystals of $Mg_3Si_2Te_6$ by self-flux method, and characterized the structure, composition, resistivity, and electronic band gap. $Mg_3Si_2Te_6$ exhibits a quasi-2D structure constituted by $Mg_2Si_2Te_6$ layers (Mg_1) that are linked by Mg_2 atoms. The single crystals can be mechanically cleaved and are sensitive to air. By combining the UV-vis absorption spectra and DFT calculations, we demonstrate that $Mg_3Si_2Te_6$ is a direct band gap semiconductor with a gap size of 1.2–1.39 eV. This gap size is close to that of silicon, and may allow $Mg_3Si_2Te_6$ become one of the candidates for NIF optoelectronic or other functional materials by tuning the energy level with rare earth ions doping. Moreover, the direct gap characteristics may provide higher photon absorption efficiency compared with traditional indirect-gap Si-based semiconductors. The absorption capacity and conversion efficiency require further investigations.

Acknowledgements

Project supported by the National Natural Science Foundation of China (Grant Nos. 12174454, 11904414, 11904416, and 12104427), the Guangdong Basic and Applied Basic Research Foundation, China (Grant No. 2021B1515120015), the Guangzhou Basic and Applied Basic Research Foundation (Grant No. 202201011123), and the National Key Research and Development Program of China (Grant No. 2019YFA0705702).

References

[1] Elliott C T 1998 *Infrared Technology and Applications XXIV* (San Diego: SPIE) pp. 763–775

[2] Maier H and Hesse J 1980 *Organic Crystals, Germanates, Semiconductors* **4** 145

[3] Bauer G and Clemens H 1990 *Semicond. Sci. Technol.* **5** S122

[4] Xie L, Wang J, Li J, Li C, Zhang Y, Zhu B P, Guo Y Z, Wang Z C and Zhang K 2021 *Adv. Electron. Mater.* **7** 2000962

[5] Zhang H D, Liu H Y, Wei K Y, Kurakevych O O, Le Godec Y, Liu Z X, Martin J, Guerrette M, Nolas G S and Strobel T A 2017 *Phys. Rev. Lett.* **118** 146601

[6] Ripka P, and Janosek M 2010 *IEEE Sensors Journal* **10** 1108

[7] Heremans J, Partin D L, Thrush C M and Green L 1993 *Semiconductor Science and Technology* **8** S424

[8] Solin S A, Thio T, Hines D R and Heremans J J 2000 *American Association for the Advancement of Science* **289** 1530

[9] Berus T, Oszwaldowski M and Grabowski J 2004 *Sensors and Actuators A: Physical* **116** 75

[10] Mihajlović G, Xiong P, Von Molnár S, Ohtani K, Ohno H, Field M and Sullivan G J 2005 *Appl. Phys. Lett.* **87** 112502

[11] Cheng P and Yang Y 2020 *Accounts of Chemical Research* **53** 1218

[12] Zheng J Y, Zhou H J, Zou Y Q, Wang R L, Lyu Yan H and Wang S Y 2019 *Energy & Environmental Science* **12** 2345

[13] Tournie E and Baranov A N 2012 *Semiconductors and Semimetals* **86** 183

[14] Harman T C and Melngailis I 1974 *Applied Solid State Science* (Amsterdam: Elsevier) pp. 1–94

[15] Downs C and Vandervelde T E 2013 *Sensors* **13** 5054

[16] Martyniuk P and Rogalski A 2008 *Progress in Quantum Electronics* **32** 89

[17] Chen W, Deng Z, Guo D Q, Chen Y J, Mazur Y I, Maidaniuk Y, Benamara M, Salamo G J, Liu H Y, Wu J and Chen B L 2018 *Journal of Lightwave Technology* **36** 2572

[18] Pasquini C 2003 *Journal of the Brazilian Chemical Society* **14** 198

[19] Li J C and Pu K Y 2003 *Chem. Soc. Rev.* **48** 38

[20] Mei L Y, Huang R F, Shen C R, Hu J G, Wang P, Xu Z J, Huang Z F and Zhu L 2003 *Adv. Opt. Mater.* **10** 2102656

[21] Rogalski A 2005 *Reports on Progress in Physics* **68** 2267

[22] Lei W, Antoszewski J and Faraone L 2015 *Appl. Phys. Rev.* **2** 041303

[23] Piotrowski J and Rogalski A 2004 *Infrared Physics & Technology* **46** 115

[24] Piotrowski J and Rogalski A 1998 *Sensors and Actuators A: Physical* **67** 146

[25] Jiao H X, Wang X D, Chen Y, Guo S F, Wu S Q, Song C Y, Huang S Y, Huang X N, Tai X C, Lin T, Shen H, Yan H, Hu W D, Meng X J, Chu J H, Zhang Y B and Wang J L 2022 *Science Advances* **8** eabn1811

[26] Yang S H, Peng J H, Huang H F, Li Z X, Dong H F and Wu F G 2022 *Materials Science in Semiconductor Processing* **144** 106552

[27] Yin J J, Wu C W, Li L S, Yu J, Sun H L, Shen B, Frandsen B A, Yao D X and Wang M 2020 *Phys. Rev. Materials* **4** 013405

[28] Sun H L, Chen C Q, Hou Y S, Wang W L, Gong Y, Huo M W, Li L S, Yu J, Cai W P, Liu N T, Wu R Q, Yao D X and Wang M 2021 *Sci. China: Phys. Mech. Astron.* **64** 118211

[29] Li L S, Hu X W, Liu Z J, Yu J, Cheng B Y, Deng S H, He L H, Cao K, Yao D X and Wang M 2021 *Sci. China: Phys. Mech. Astron.* **64** 287412

[30] Perdew J P, Burke K and Ernzerhof M 1996 *Phys. Rev. Lett.* **77** 3865

[31] Vargas Hernández R A 2020 *J. Phys. Chem. A* **124** 4053

[32] Carteaux V, Brunet D, Ouvrard G and Andre G 1995 *J. Phys.: Condens. Matter* **7** 69

[33] Cai W P, Sun H L, Xia W, Wu C W, Liu Y, Liu H, Gong Y, Yao D X, Guo Y F and Wang M 2020 *Phys. Rev. B* **102** 144525

[34] Vincent H, Leroux D, Bijaoui D, Rimet R and Schlenker C 1986 *Journal of Solid State Chemistry* **63** 349

[35] May A F, Cao H B and Calder S 2020 *J. Magn. Magnet. Mater.* **511** 166936

[36] Ni Y F, Zhao H D, Zhang Y, Hu B, Kimchi I and Cao G 2021 *Phys. Rev. B* **103** L161105

[37] Seo J, De C, Ha H, Lee J E, Park S, Park J, Skourski Y, Choi E S, Kim B and Cho G Y, Yeom H W, Cheong S W, Kim J H, Yang B J, Kim K and Kim J S 2021 *Nature* **599** 576

[38] Wang Z, Xia H, Wang P, et al. 2021 *Adv. Mater.* **33** 2104942

[39] Chen J W, Li L, Gong P L, Zhang H L, Yin S Q, Li M, Wu L F, Gao W S, Long M S, Shan L, Yan F, and Li G H 2022 *ACS Nano* **16** 7745

[40] Sarkar A, Loho C, Velasco L, Thomas T, Bhattacharya S S, Hahn H, and Djenadic R 2017 *Dalton Transactions* **46** 12167

[41] Tauc J, Grigorovici R and Vancu A 1966 *Physica Status Solidi (b)* **15** 627